Article:
Wang, H., Liu, J., Klaar, M. orcid.org/0000-0001-8920-4226 et al. (3 more authors) (2024) Anthropogenic climate change has influenced global river flow seasonality. Science, 383 (6686). pp. 1009-1014. ISSN 0036-8075

https://doi.org/10.1126/science.adi9501

Anthropogenic climate change has influenced global river flow seasonality

Hong Wang[1,2], Junguo Liu[1,3,4*], Megan Klaar[2], Aifang Chen[1], Lukas Gudmundsson[5], Joseph Holden[2]

Affiliations:

[1]School of Environmental Science and Engineering, Southern University of Science and Technology, Shenzhen, 518055, China

[2]water@leeds, School of Geography, University of Leeds, Leeds, LS2 9JT, UK

[3]North China University of Water Resources and Electric Power, Zhengzhou, China

[4]Henan Provincial Key Lab of Hydrosphere and Watershed Water Security, North China University of Water Resources and Electric Power, Zhengzhou, China

[5]Institute for Atmospheric and Climate Science, ETH Zürich, Zürich, Switzerland

*Correspondence: e-mail: liujg@sustech.edu.cn

Abstract: Riverine ecosystems have adapted to natural discharge variations across seasons. However, evidence suggesting that climate change has already impacted magnitudes of river flow seasonality is limited to local studies, mainly focusing on changes of mean or extreme flows. This study introduces the use of apportionment entropy as a robust measure to assess flow volume non-uniformity across seasons, enabling a global analysis. We find ~21% of long-term river gauging stations exhibit significant alterations in seasonal flow distributions, but two thirds of these are unrelated to trends in annual mean discharge. By combining a data-driven runoff reconstruction with state-of-the-art hydrological simulations, we identify a discernible weakening of river flow seasonality in northern high latitudes (above 50°N), a phenomenon directly linked to anthropogenic climate forcing.

One-Sentence Summary: We find that differences in monthly river flow distributions are reduced in northern high latitudes, a phenomenon adequately explained by climate models only when anthropogenic climate change is accounted for.

Anthropogenic climate warming, which could drive changes in the hydrological cycle, has received increasing attention (*1*). Water availability, a key concern, is directly related to ecosystem functions and societal interactions (*2*, *3*). However, human activities are altering river flow patterns worldwide, both directly through flow regulations, and indirectly through land use change and the impacts of anthropogenic climate change (ACC) on air temperature, precipitation, soil moisture, and snowmelt regimes (*4–6*). Consequently, over two-thirds of the world's rivers have been altered even without considering the indirect impacts from ACC, characterized by human-induced alterations in greenhouse gases and aerosols (*7*).

River flow seasonality (RFS) plays a critical role in floods and droughts, threatening water security and freshwater biodiversity (*4*, *8*). For example, a substantial portion of the early meltwater from snowpack depletion may ultimately flow into oceans without being available for human use (*9*). In addition, weakening RFS (e.g., flood frequency reduction) can greatly simplify community-wide riparian plant networks (*10*, *11*). Riparian vegetation subsequently influences freshwater biota to make seasonal use of riparian areas and floodplains for feeding or breeding purposes (*12*).

Recent studies have shown a tendency for changes in RFS from timing or magnitude perspectives (*5*, *6*, *13*). However, these studies either lack global representativeness or fail to consider the impact of ACC explicitly. Nonetheless, there is growing evidence that ACC has influences on seasonal river flow, as indicated by climate and hydrological model simulations (*14*, *15*). Moreover, human-induced seasonal changes were detected in the western United States (*16*). However, the question of whether ACC is detectable in the magnitude of RFS at global scales remains unanswered, and it is challenging to transfer the evidence across regions since river flow may vary locally due to atmospheric, oceanic, and terrestrial modulation (*17*).

Here we use *in situ* observations of monthly average river flow (*18*) from 10,120 gauging stations with either a minimum data length of 35 years or uncertainty-controlled shorter records from 1965 to 2014. In addition, we employ recently published datasets of observation-based global gridded runoff (GRUN) reconstructed from data-driven models calibrated with observations to achieve global scale coverage (*19*). Multimodel results from the Inter-Sectoral Impact Model Intercomparison Project phase 2b (ISIMIP2b) are presented for detecting and attributing observed changes to human influences on the climate system (*20*). To inform our global analysis of seasonal flow regimes, a generalized seasonality index was developed using apportionment entropy (AE) (*21*). AE non-parametrically quantifies how evenly flow rates are distributed across months, where a large AE indicates a uniform distribution (low RFS) and low AE points to large month to month differences (high RFS). AE can be used to characterize changes in a hydro-climatological context because it is statistically well suited to the characteristics of highly variable flow regimes (*21*, *22*).

Changes in the trend of river flow seasonality

The northern high latitudes (above 50°N) showed discernible weakening in the seasonal cycle of river flow (increasing AE, fig. S1) (Fig. 1). In northern North America (N. NA), ~40% of stations showed significant decreasing RFS ($p < 0.05$). In comparison, only ~2% showed significant increasing trends of RFS. Similar results are also observed in south Siberia (S. SI) with ~32% of stations showing significant decreasing seasonality and only ~1% of stations showing significant increasing seasonality. We further found a comparable pattern in Europe (EU) with ~19% of the stations significantly experiencing decreasing RFS mainly located in northern Europe (N. EU), western Russia (W. RU), and the European Alps, while ~4% showed significantly increasing RFS, mainly concentrated downstream of the Alps (Fig. 1C). In addition, regions in the contiguous United States (CONUS) present predominantly decreasing trends of RFS overall, except for rivers in the Rocky Mountains and Florida in the

western and eastern CONUS, respectively. In central North America (C. NA), significant decreasing RFS trends account for ~18% of stations in contrast with 4% showing significant increasing RFS trends (Fig. 1D). Western Russia, upper Midwest (U. Midwest), and south Siberia (S. SI) display greater changes in magnitude for RFS trends. While more than half of the stations in the northern high latitudes showed no statistically significant ($p > 0.05$) trends, both the significant and non-significant trends tell the same story, that is, RFS decreased in the northern high latitudes. Contrary to the results, increasing RFS was observed in ~25% of the stations in southeast Brazil (S. BR) versus ~4% with decreasing RFS. Global patterns in seasonality trends during the more recent period of 1970-2019 generally agree with the trends computed for the 1965-2014 time frame (fig. S2). However, it should be noted that some spatial resolution is lost when we use the 1970-2019 time window, for example, in western Russia, because data are not available for sufficient length.

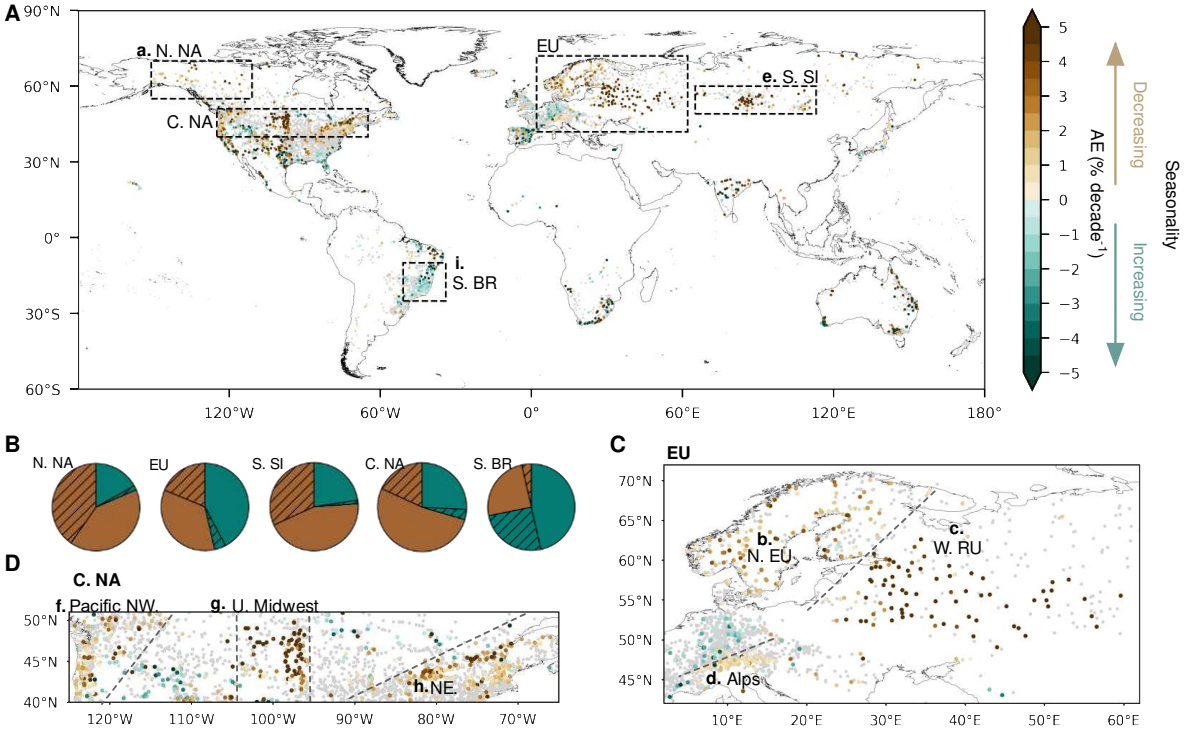

Fig. 1: River flow seasonality (RFS) trends represented by apportionment entropy (AE) (% decade^{-1}) over 50 years (1965–2014). (**A**) Map shows stations with significant RFS trends ($p < 0.05$), where green and brown colours represent increasing (decreasing) and decreasing (increasing) RFS (AE) trends, respectively. Stations with non-significant changes ($p > 0.05$) are presented as smaller grey dots. The five boxes mark the regions of interest: northern North America (a. N. NA), Europe (EU), south Siberia (e. S. SI), central North America (C. NA), and southeast Brazil (i. S. BR). (**B**) Pie charts show the distribution of significant ($p < 0.05$; hatched) and non-significant ($p > 0.05$; solid) trends, corresponding to the direction of increasing (green) and decreasing (brown) RFS trends in five boxed regions. (**C, D**) Subareas in EU (C) and C. NA (D) dominated by the same AE change direction are delimitated by dashed grey lines: northern Europe (b), western Russia (c), the high elevation Europe Alps (d), Pacific northwest (f), upper Midwest (g), and northeast CONUS (h). Significance is estimated by the Mann-Kendal trend test.

Monthly high and low flow changes mediate seasonality

For better interpretation of seasonal variations, AE trends were combined with annual mean river flow trends (fig. S3A) to divide stations into six types (Fig. 2). For each station, we

define low flow months as the three calendar months with lowest long-term monthly mean river flow, while high-flow months are the three calendar months with greatest monthly mean flow. Therefore, trends in low- and high- flow months (T_{LH}) contribute to annual mean and seasonal variations of river flow. We found seasonal variations in the northern high latitudes to be dominated by increasing low flows and decreasing high flows (L+H−; increasing trends of low flows and decreasing trends of high flows) accounting for ~46% of sites and increasing low flows solely (L+H*; increasing trends of low flows and non-prominent changes in high flows) accounting for ~14% of stations. These two patterns result in a significant decrease in RFS with no significant annual mean trends (L+H−) or significant increasing annual mean trends (L+H*). The distribution of the two patterns agrees with broad-scale climate trends in snowmelt-dominated regions (northern North America, northern Europe, western Russia, south Siberia, higher elevation European Alps, upper Midwest, and northeast CONUS) (Fig. 2). Out of 1137 stations in the snowmelt-dominated areas (grey regions in Fig. 2A), 979 are experiencing significant weakening RFS. Around 30% of river gauges displayed significantly increasing RFS and prominent low flow decreases, herein represented as L−H* (~12%; decreasing trends of low flows and non-prominent changes of high flows) and L−H+ (~18%; decreasing trends of low flows and increasing trends of high flows), such as in Florida and the Rocky Mountains in the CONUS, lower catchments of the European Alps, and southeast Brazil. A smaller number of sites experienced changes in high-flow months, including L*H+ (~2%; non-prominent changes of low flows and increasing trends of high flows) and L*H− (~8%; non-prominent changes of low flows and decreasing trends of high flows), suggesting high flows alone play a minor role in influencing RFS trends.

Overall, the majority of stations showed L+H− and L−H+ (~65%), indicating low and high flows interact to affect seasonality and mask annual mean trends of river flow (see also fig. S3B). Moreover, the proportion of sites (L−H* and L+H*; ~26%) where low flow variations are the predominant factor is double that of high flows (L*H+ and L*H−; ~9%), highlighting the key role that low flow changes played in the AE shifts. Trends of annual low- and high-flows are analyzed separately in fig. S4, supporting our findings that increasing river flow in low-flow months are contributing to weakening RFS in the snowmelt-dominated areas.

Our results are consistent with other studies that have explored seasonal trends at regional scales. For example, earlier timing and reduced flood magnitude have been observed in northern Europe, western Russia, and the European Alps (*5*, *6*). Previous studies also support findings of stations facing increasing RFS. For instance, the frequency of low-flow events increased in the low-flow spring season (*23*), corresponding to the spreading of L−H+ and L−H* categories. In the Rocky Mountains region (CONUS), early snowmelt can reduce river flow in low-flow months due to less extensive spring snow cover (L−H*) aligning with ref. (*11*). Moreover, stations characterized by L−H+, such as those in southeast Brazil, suggest a high risk of hazards from both drought and flood events aligning with ref. (*24*, *25*).

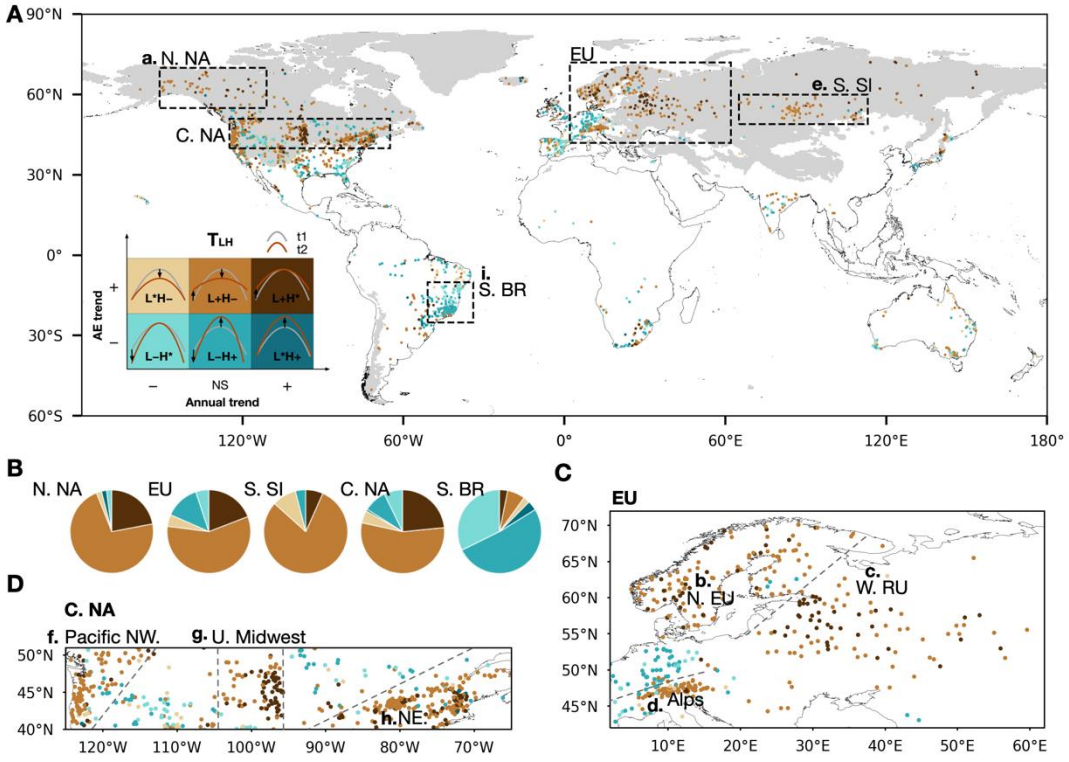

Fig. 2: Classification of potential reasons for changes in river flow seasonality. (**A**) Spatial distribution of trend directions in low flows and high flows (T_{LH}) indicated by change directions of apportionment entropy (AE) and annual mean river flow (NS: insignificant). Character * indicates no predominant changes of low flows or high flows. Labels show illustrations of flow regime changes from period t1 to t2, corresponding to six types of T_{LH}. The five boxes mark the regions of interest: northern North America (a. N. NA), Europe (EU), south Siberia (e. S. SI), central North America (C. NA), and southeast Brazil (i. S. BR). (**B**) Pie charts show the proportion of T_{LH} in five boxed regions in panel (A). (**C, D**) subareas in EU (C) and C. NA (D) with the same AE change direction are delimitated by dashed grey lines: northern Europe (b), western Russia (c), the high elevation Europe Alps (d), Pacific northwest (f), upper Midwest (g), and northeast CONUS (h). Regions where snow fraction in precipitation is larger than 0.2 are showed in grey as snowmelt-dominated areas in panel (A).

Regional seasonality changes and potential mechanisms

To understand the change of RFS trends regionally, we focused on annual mean and monthly river flow trends and normalized flow regimes in nine hotspots (fig. S5). Increasing trends were most pronounced in low-flow months except in southeast Brazil, in agreement with a large proportion of L+H− and L+H* stations (Fig. 2). This suggests that the upper limit of the environmental flow envelopes is increasingly being exceeded during low-flow months in high latitudes (*26*). To interpret potential mechanism of RFS trends, we chose subspaces of nine hotspots for a finer analysis (fig. S6). In snow-dominated regions, decreasing snow fraction corresponding to snow-rain transition and snowpack depletion plays a more important role in shaping RFS than precipitation. Warmer temperatures can deplete snowpacks, contributing to greater frequency of high-flow events and lower frequency of low-flow events prior to the normal flood season, and hence reducing monthly differences in river flow (*5*, *23*). Early spring greening, closely related to early spring snowmelt, can exacerbate soil moisture deficits in spring and summer (high-flow months in snow-dominated areas) (e.g., the Alps, fig. S6) (*27*). This can indirectly dampen river flow regimes by

reducing runoff generation in high-flow months. However, decreasing RFS can also coincide with increasing soil moisture in high-flow months (e.g., western Russia, fig. S6). More precipitation falling as rain when air temperatures are around freezing are associated with shallower snowpacks and likely increased infiltration resulting from less frozen upper soil layers, and therefore lead to a rise in soil moisture and smaller floods in the spring flood season (*5*). Soil moisture initially decreased before increasing in northern North America, northeast CONUS and south Siberia, indicating a shift of primary driving factor (fig. S6). Additionally, permafrost mass loss may continue to generate runoff thereafter (e.g., south Siberia, fig. S5E) (*28*).

Precipitation plays a more important role in RFS in nonsnowmelt-dominated regions. For instance, seasonality of precipitation and river flow are positively correlated (table S1, Spearman rank correlation coefficients of $r = 0.65$) due to the dominance of rain in the coast of Pacific Northwest (fig. S6) (*23*). Similarly, increased RFS are associated with increased precipitation seasonality in southeast Brazil (table S1, $r = 0.93$) (fig. S6), in agreement with ref. (*29*). We notice the majority of stations in the Pacific Northwest show increasing monthly river flow in the late spring and summer contradicting the findings of previous studies (fig. S5F) (*4*, *30*). The reason for the difference between results may be due to varied El Niño Southern Oscillation (ENSO) impacts in different study periods (*31*). Temperature anomalies in ENSO phases strongly influence precipitation and snow accumulation and in turn affect spring and summer river flow.

Climate change detection and attribution analysis of RFS trends

To investigate whether ACC caused the consistent decreasing trends of RFS in northern high latitudes, we augment the assessment of in-situ observations with an analysis of the observation-based global runoff reconstruction (GRUN) to obtain a comprehensive spatial and temporal representation of RFS trends (*19*). The reconstructed spatial trend patterns of AE are compared with the corresponding trend pattern estimated by a multimodel ensemble mean of 27 simulations from global hydrological models (GHMs) (*20*). These GHMs considering human water and land use (HWLU) are driven by atmospheric data from climate models that account for historical radiative forcing (HIST) (abbreviated as HIST&HWLU) (*20*). Overall, the simulated trends are consistent with the reconstruction, highlighting that the GHM simulations generally capture the observed changes (Fig. 3A, 3B and 3D). Simulations from GHMs also show a general agreement above 50°N that supports the spatial pattern of RFS changes (fig. S7). Some differences are expected between the multimodel mean and observations. For example, the magnitude of AE trends is weaker in the multimodel mean. This weaker magnitude is most likely due to the averaging across the ensemble that reduces the effects of internal variability in the climate forcing, while the GRUN reconstruction represents a single observed evolution of the system (*32*). Note that GRUN does not account for the effects of HWLU, which possibly cause some differences in the magnitude of AE trends. In addition, the high uncertainties of GRUN reconstruction and multimodel simulations possibly contribute to the disagreement in the Arctic region of north Canada. However, the simulated trends in AE derived from GHMs that account for HWLU and are driven with atmospheric variables from pre-industrial control climate models simulations (Picontrol&HWLU) fail to capture the observed changes (Fig. 3C and 3D), indicating that HWLU is not contributing to the weakening pattern of RFS. Analyses from 1970-2019 showed the same trends in RFS indicating that simulations are consistent with observations only when ACC is considered (figs. S8 and S9).

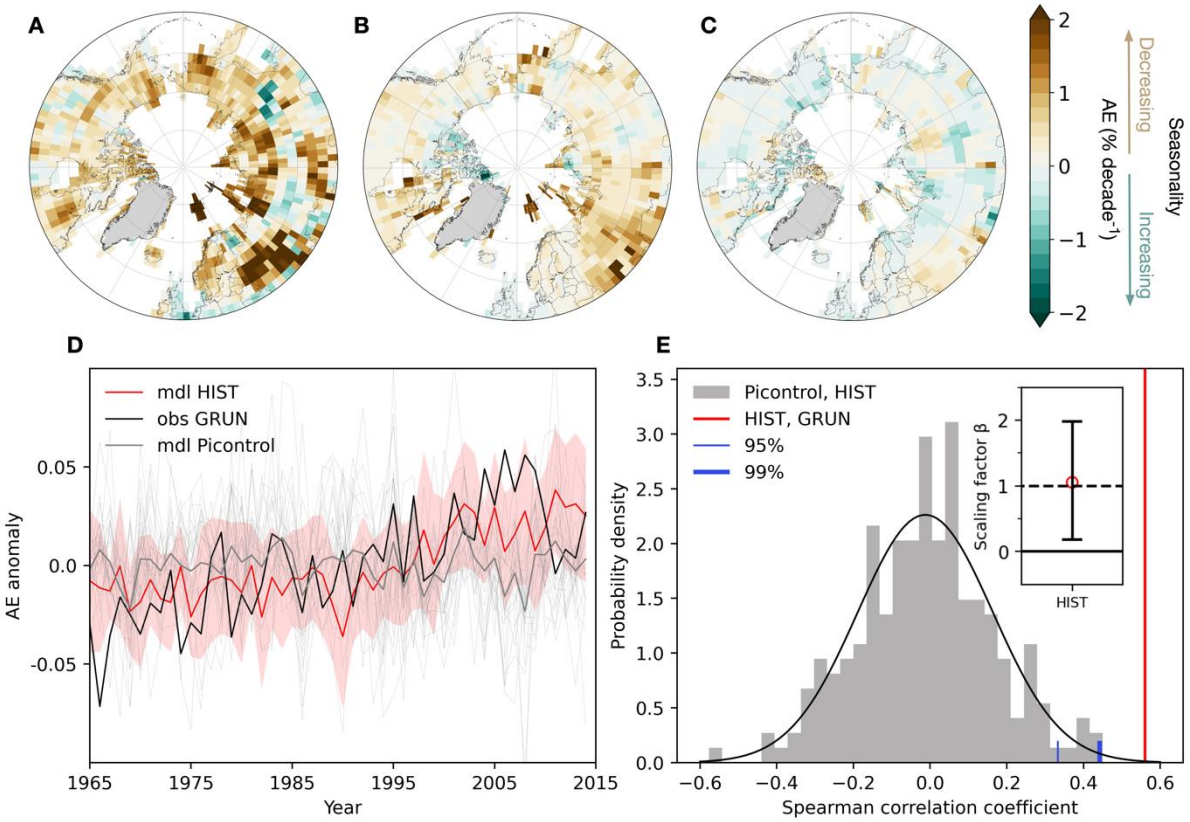

Fig. 3: Comparison of apportionment entropy (AE) trends from observation-based reconstructions and global hydrological models for 1965-2014 (% decade^{-1}) in the northern high latitudes (above 50°N). (**A**) Reconstruction from GRUN. (**B, C**) Simulated changes based on multimodel mean that account for historical water and land use (HWLU) under the effects of either historical radiative forcing accounting for human-induced emissions (HIST) (B), or pre-industrial climate forcing (Picontrol) on atmospheric variables (C). Areas with annual precipitation below 100 mm and Greenland are masked in grey. (**D**) Multimodel (mdl) mean time series of annual apportionment entropy (AE) anomalies for HIST&HWLU and Picontrol&HWLU response and GRUN observations averaged for the northern high latitudes (above 50°N). The red spread is ensemble standard deviation of HIST&HWLU, and thin grey lines are 27 model results of Picontrol&HWLU. (**E**) Correlations of AE anomalies between simulations with and without ACC ($corr_{temporary}$(Picontrol, HIST)) or observation-based reconstruction ($corr_{temporary}$(HIST, GRUN)) across 50°N-90°N. Spearman correlations between the mdl mean from HIST&HWLU simulations and 216 chunks of Picontrol simulations with 50-yr segments are shown as an empirical probability density function in grey. Vertical blue lines mark the 95% and 99% cumulative probability of an assumed normal distribution for the correlations. The inset shows the confidence interval of scaling factor plot from optimal fingerprinting method with 0.5-99.5% uncertainty range. A signal is detected if the lower confidence bound is above zero (the solid line). The amplitude of the mean response is consistent with the observations if the confidence interval includes one (the dashed line). The residual consistency test (RCT) passed ($p > 0.1$), indicating the consistency between the regression residuals and the model-simulated variability.

To quantitatively assess the influence of ACC on the observed spatial pattern and temporal evolution of RFS across northern high latitudes, correlation based (*17*, *32*, *33*) and optimal fingerprinting methods (*17*, *33*, *34*) were used to test against the null hypothesis that there is

no detectable pattern of AE trends in the observations resulting from ACC. The correlation approach uses all available AE trends and anomalies of simulations under HIST&HWLU and Picontrol (table S2). The spatial correlations between HIST simulations and a large ensemble of the Picontrol simulations were calculated from the multimodel simulation mean of AE trends forced with HIST and every chunk (216 estimates) of AE trends with Picontrol conditions (fig. S10). There is a 95% probability that the spatial Spearman correlations between multimodel mean of HIST simulations and GRUN ($corr_{spatial}$(HIST, GRUN)) are greater than what is expected from Picontrol simulations ($corr_{spatial}$(Picontrol, HIST)). This strongly suggests that ACC is the underlying cause for the spatial pattern of RFS. In addition, the temporal correlation of AE anomalies between multimodel mean of HIST simulations and GRUN ($corr_{temporary}$(HIST, GRUN)) is larger than for all correlations from Picontrol versus HIST ($corr_{temporary}$(Picontrol, HIST)) at 99% confidence level (Fig. 3E). These findings further confirm that human-induced emissions contribute to the decrease in RFS in the northern high latitudes.

An additional test employed regularized optimal fingerprinting (*34*). Observations (y) are regressed on the multimodel mean of the simulation forced with HIST&HWLU (x) while considering sampling error $\boldsymbol{\nu}$ and natural variability derived from Picontrol&1860soc ($\boldsymbol{\varepsilon}$): $y = \boldsymbol{\beta}\,(x - \boldsymbol{\nu}) + \varepsilon$. The inset in Fig. 3E displays the scaling factor $\boldsymbol{\beta}$ at 99% confidence level of scaling factor above 0 in the experiment of HIST, suggesting that the considered simulations capture the observed AE changes when human-influenced climate changes are taken into account. Furthermore, the confidence interval of scaling factor $\boldsymbol{\beta}$ under HIST includes one, which implies that the magnitude of the simulated trend is consistent with the observations. Moreover, a residual consistency test (RCT) did not indicate an inconsistency between the regression residuals and the model-simulated variability ($p > 0.1$). An overall climate change detection and attribution analysis for 1970-2019 provides further evidence that human-induced emissions continue to contribute to decreased RFS in the northern high latitudes (fig. S11). The primary climate change detection and attribution assessment that focuses on the northern high latitudes to optimize the signal-to-noise ratio is complemented with regional assessment (fig. S12). Changes of RFS were captured with 10-90% confidence intervals in Alaska, northern Europe and northern Asia defined by IPCC SREX (Intergovernmental Panel on Climate Change Special Report on Extreme events) only if ACC is considered. These results confirm the robustness of our conclusions regarding the influence of ACC on the temporal evolution of RFS in the northern high latitudes. Seasonality changes are also detected by model simulations that account for anthropogenic emissions in central America, southern Africa, and east Asia. This finding implies that human-induced emissions potentially exert an influence on the seasonality of monsoon precipitation and consequent runoff dynamics.

We acknowledge that human interference, such as flow regulation through reservoirs, may also contribute to RFS changes (*35*). Importantly, however, we note that over three-fifths of the *in-situ* observations, which are free from reservoir flow regulation (located in the subbasins with zero degree of regulation), exhibit the same spatial pattern of RFS trends as identified in our global dataset (fig. S13). Moreover, an observational reconstruction runoff derived from GRUN, which is free from human interference (including reservoirs, human water management, and land use change), demonstrates a similar trend to that observed at the stations, though with smaller magnitudes of RFS trends (fig. S14). Moreover, simulations replicating pre-industrial climate conditions but considering historical human activities (Picontrol&HWLU) fail to reproduce the trend of RFS in the northern high latitudes. Combining the climate change detection and attribution analysis for grid cells where direct observation data are available robustly shows that ACC contributes to the weakening of RFS

in the northern high latitudes (fig. S15). We also note that historical natural climate forcing (i.e., solar, volcanic activity) is not excluded when using ISIMIP2b to undertake the climate change detection and attribution analysis (*36*). Nonetheless, natural climate forcing has a limited impact on river flow due to much smaller solar changes compared with ACC (*37*) and short-lived influence of volcanic eruptions (*38*). Furthermore, no significant trends of precipitation seasonality have been observed in the northern high latitudes, demonstrating that precipitation seasonality change cannot account for our results (fig. S16). It is likely that observed rain–snow transition and increasing snowmelt under global warming led to a weakening trend of RFS in the northern high latitudes (fig.S6 and table S1). The underlying physics behind this assertion is temperature-driven rather than precipitation-driven, and ACC is acknowledged to far surpass natural forcing in dominating a warming future (*37*).

Our findings present changes in the seasonal cycles of river flow by adapting an AE perspective, and clearly demonstrate that decreased RFS is attributable to ACC in the northern high latitudes. Possible climatic mechanisms that might drive flow regime dampening above 50°N under ACC include early snowpack depletion (*23*), loss of glacier extent (*39*), permafrost loss (*40*), increasing proportion of precipitation as rainfall (*41*) and shorter freezing periods (*42*, *43*) interacting with ocean–atmosphere oscillations (*31*). Depending on the region, some of these drivers can be more important than others in explaining RFS changes.

This study provides a standpoint for understanding changing seasonal patterns of river flow. There is an increasing need for accelerated climate adaptation efforts to safeguard freshwater ecosystems, achieved through e.g., use of managed environmental flows (*8*). Additionally, these efforts are essential for establishing sustainable water resource management by identifying and mitigating risks related to flood and drought, exploring seasonal storage opportunities, and optimizing allocations for irrigation or hydropower generation (*4*, *44*). It should be noted that water management might synergistically contribute to RFS dampening (*35*, *45*). Therefore, it is essential to develop mitigation strategies and adaptation planning to alleviate the future homogenization of seasonal river flow, particularly in locations such as European Russia, Scandinavia, and Canada.

References

1. P. Wu, N. Christidis, P. Stott, Anthropogenic impact on Earth's hydrological cycle. *Nat. Clim. Chang*. **3**, 807–810 (2013).
2. C. J. Vörösmarty, P. Green, J. Salisbury, R. B. Lammers, Global water resources: Vulnerability from climate change and population growth. *Science*. **289**, 284–288 (2000).
3. P. C. D. Milly, K. A. Dunne, A. V. Vecchia, Global pattern of trends in streamflow and water availability in a changing climate. *Nature*. **438**, 347–350 (2005).
4. N. K. Singh, N. B. Basu, The human factor in seasonal streamflows across natural and managed watersheds of North America *Nat. Sustain.* **5**, 397-405 (2022), doi:10.1038/s41893-022-00848-1.
5. G. Blöschl, J. Hall, A. Viglione, R. A. P. Perdigão, J. Parajka, B. Merz, D. Lun, B. Arheimer, G. T. Aronica, A. Bilibashi, M. Boháč, O. Bonacci, M. Borga, I. Čanjevac, A. Castellarin, G. B. Chirico, P. Claps, N. Frolova, D. Ganora, L. Gorbachova, A. Gül, J. Hannaford, S. Harrigan, M. Kireeva, A. Kiss, T. R. Kjeldsen, S. Kohnová, J. J. Koskela, O. Ledvinka, N. Macdonald, M. Mavrova-Guirguinova, L. Mediero, R. Merz, P. Molnar, A. Montanari, C. Murphy, M. Osuch, V. Ovcharuk, I. Radevski, J. L. Salinas, E. Sauquet, M. Šraj, J. Szolgay, E. Volpi, D. Wilson, K. Zaimi, N. Živković, Changing climate both increases and decreases European river floods. *Nature*. **573**, 108–111 (2019).
6. G. Blöschl, J. Hall, J. Parajka, R. A. P. Perdigão, B. Merz, B. Arheimer, G. T. Aronica, A. Bilibashi, O. Bonacci, M. Borga, I. Čanjevac, A. Castellarin, G. B. Chirico, P. Claps, K. Fiala, N. Frolova, L. Gorbachova, A. Gül, J. Hannaford, S. Harrigan, M. Kireeva, A. Kiss, T. R. Kjeldsen, S. Kohnová, J. J. Koskela, O. Ledvinka, N. Macdonald, M. Mavrova-Guirguinova, L. Mediero, R. Merz, P. Molnar, A. Montanari, C. Murphy, M. Osuch, V. Ovcharuk, I. Radevski, M. Rogger, J. L. Salinas, E. Sauquet, M. Šraj, J. Szolgay, A. Viglione, E. Volpi, D. Wilson, K. Zaimi, N. Živković, Changing climate shifts timing of European floods. *Science*. **357**, 588–590 (2017).
7. M. Dynesius, C. Nilsson, Fragmentation and flow regulation of river systems in the northern third of the world. *Science*. **266**, 753-762 (1994).
8. M. Palmer, A. Ruhi, Linkages between flow regime, biota, and ecosystem processes: Implications for river restoration. *Science*. **365** (2019), doi:10.1126/science.aaw2087.
9. T. P. Barnett, J. C. Adam, D. P. Lettenmaier, Potential impacts of a warming climate on water availability in snow-dominated regions. *Nature.* **438**, 303–309 (2005).
10. J. D. Tonkin, D. M. Merritt, J. D. Olden, L. V. Reynolds, D. A. Lytle, Flow regime alteration degrades ecological networks in riparian ecosystems. *Nat. Ecol. Evol*. **2**, 86–93 (2018).
11. S. B. Rood, J. Pan, K. M. Gill, C. G. Franks, G. M. Samuelson, A. Shepherd, Declining summer flows of Rocky Mountain rivers: Changing seasonal hydrology and probable impacts on floodplain forests. *J. Hydrol.* **349**, 397–410 (2008).
12. H. L. Bateman, D. M. Merritt, Complex riparian habitats predict reptile and amphibian diversity. *Glob. Ecol. Conserv*. **22**, 1–10 (2020).
13. C. Wasko, R. Nathan, M. C. Peel, Trends in Global Flood and Streamflow Timing Based on Local Water Year. *Water Resour. Res*. **56**, 1–12 (2020).
14. S. Eisner, M. Flörke, A. Chamorro, P. Daggupati, C. Donnelly, J. Huang, Y. Hundecha, H. Koch, A. Kalugin, I. Krylenko, V. Mishra, M. Piniewski, L. Samaniego, O. Seidou, M. Wallner, V. Krysanova, An ensemble analysis of climate change impacts on streamflow seasonality across 11 large river basins. *Clim. Change*. **141**, 401–417 (2017).

15. K. Marvel, B. I. Cook, C. Bonfils, J. E. Smerdon, A. P. Williams, H. Liu, Projected Changes to Hydroclimate Seasonality in the Continental United States. *Earth's Future*. **9**, 1–19 (2021).
16. T. P. Barnett, D. W. Pierce, H. G. Hidalgo, C. Bonfils, B. D. Santer, T. Das, G. Bala, A. W. Wood, T. Nozawa, A. A. Mirin, D. R. Cayan, M. D. Dettinger, Human-induced changes in the hydrology of the Western United States. *Science*. **319**, 1080–1083 (2008).
17. L. Gudmundsson, S. I. Seneviratne, X. Zhang, Anthropogenic climate change detected in European renewable freshwater resources. *Nat. Clim. Chang*. **7**, 813–816 (2017).
18. H. X. Do, L. Gudmundsson, M. Leonard, S. Westra, The Global Streamflow Indices and Metadata Archive (GSIM)-Part 1: The production of a daily streamflow archive and metadata. *Earth Syst. Sci. Data*. **10**, 765–785 (2018).
19. G. Ghiggi, V. Humphrey, S. I. Seneviratne, L. Gudmundsson, GRUN: An observation-based global gridded runoff dataset from 1902 to 2014. *Earth Syst. Sci. Data*. **11**, 1655–1674 (2019).
20. K. Frieler, S. Lange, F. Piontek, C. P. O. Reyer, J. Schewe, L. Warszawski, F. Zhao, L. Chini, S. Denvil, K. Emanuel, T. Geiger, K. Halladay, G. Hurtt, M. Mengel, D. Murakami, S. Ostberg, A. Popp, R. Riva, M. Stevanovic, T. SuzGBRi, J. Volkholz, E. Burke, P. Ciais, K. Ebi, T. D. Eddy, J. Elliott, E. Galbraith, S. N. Gosling, F. Hattermann, T. Hickler, J. Hinkel, C. Hof, V. Huber, J. Jägermeyr, V. Krysanova, R. Marcé, H. Müller Schmied, I. Mouratiadou, D. Pierson, D. P. Tittensor, R. Vautard, M. van Vliet, M. F. Biber, R. A. Betts, B. L. Bodirsky, D. Deryng, S. Frolking, C. D. Jones, H. K. Lotze, H. Lotze-Campen, R. Sahajpal, K. Thonicke, H. Tian, Y. Yamagata, Assessing the impacts of 1.5°C global warming - simulation protocol of the Inter-Sectoral Impact Model Intercomparison Project (ISIMIP2b). *Geosci. Model Dev*. **10**, 4321–4345 (2017).
21. X. Feng, A. Porporato, I. Rodriguez-Iturbe, Changes in rainfall seasonality in the tropics. *Nat. Clim. Chang*. **3**, 811–815 (2013).
22. G. Konapala, A. K. Mishra, Y. Wada, M. E. Mann, Climate change will affect global water availability through compounding changes in seasonal precipitation and evaporation. *Nat. Commun*. **11**, 1–10 (2020).
23. E. N. Dethier, S. L. Sartain, C. E. Renshaw, F. J. Magilligan, Spatially coherent regional changes in seasonal extreme streamflow events in the United States and Canada since 1950. *Sci. Adv*. **6** (2020), doi:10.1126/sciadv.aba5939.
24. M. R. Viola, C. R. de Mello, S. C. Chou, S. N. Yanagi, J. L. Gomes, Assessing climate change impacts on Upper Grande River Basin hydrology, Southeast Brazil. *Int. J. Climatol*. **35**, 1054–1068 (2015).
25. D. Bartiko, D. Y. Oliveira, N. B. Bonumá, P. L. B. Chaffe, Spatial and seasonal patterns of flood change across Brazil. *Hydrol. Sci. J*. **64**, 1071–1079 (2019).
26. V. Virkki, E. Alanärä, M. Porkka, L. Ahopelto, T. Gleeson, C. Mohan, L. Wang-Erlandsson, M. Flörke, D. Gerten, S. N. Gosling, N. Hanasaki, H. Müller Schmied, N. Wanders, M. Kummu, Globally widespread and increasing violations of environmental flow envelopes, Globally widespread and increasing violations of environmental flow envelopes. *Hydrol. Earth Syst. Sci*. **26**, 3315–3336 (2022).
27. X. Lian, S. Piao, L. Z. X. Li, Y. Li, C. Huntingford, P. Ciais, A. Cescatti, I. A. Janssens, J. Peñuelas, W. Buermann, A. Chen, X. Li, R. B. Myneni, X. Wang, Y. Wang, Y. Yang, Z. Zeng, Y. Zhang, T. R. McVicar, Summer soil drying exacerbated by earlier spring greening of northern vegetation. *Sci. Adv*. **6**, 1–12 (2020).
28. E. Gautier, T. Dépret, F. Costard, C. Virmoux, A. Fedorov, D. Grancher, P. Konstantinov, D. Brunstein, Going with the flow: Hydrologic response of middle Lena River (Siberia) to the climate variability and change. *J. Hydrol.* **557**, 475–488 (2018).

29. V. B. P. Chagas, P. L. B. Chaffe, G. Blöschl, Process Controls on Flood Seasonality in Brazil. *Geophys. Res. Lett*. **49**, 1–10 (2022).
30. P. W. Mote, S. Li, D. P. Lettenmaier, M. Xiao, R. Engel, Dramatic declines in snowpack in the western US. *NPJ Clim. Atmos. Sci*. **1** (2018), doi:10.1038/s41612-018-0012-1.
31. D. Lee, P. J. Ward, P. Block, Identification of symmetric and asymmetric responses in seasonal streamflow globally to ENSO phase. *Environ. Res. Lett*. **13** (2018), doi:10.1088/1748-9326/aab4ca.
32. R. S. Padrón, L. Gudmundsson, B. Decharme, A. Ducharne, D. M. Lawrence, J. Mao, D. Peano, G. Krinner, H. Kim, S. I. Seneviratne, Observed changes in dry-season water availability attributed to human-induced climate change. *Nat. Geosci*. **13**, 477–481 (2020).
33. L. Grant, I. Vanderkelen, L. Gudmundsson, Z. Tan, M. Perroud, V. M. Stepanenko, A. V Debolskiy, B. Droppers, A. B. G. Janssen, R. I. Woolway, M. Choulga, G. Balsamo, G. Kirillin, J. Schewe, F. Zhao, I. V. del Valle, M. Golub, D. Pierson, R. Marcé, S. I. Seneviratne, W. Thiery, Attribution of global lake systems change to anthropogenic forcing. *Nat Geosci* **14**, 849–854 (2021).
34. A. Ribes, S. Planton, L. Terray, Application of regularised optimal fingerprinting to attribution. Part I: Method, properties and idealised analysis. *Clim. Dyn*. **41**, 2817–2836 (2013).
35. B. Arheimer, C. Donnelly, G. Lindström, Regulation of snow-fed rivers affects flow regimes more than climate change. *Nat. Commun*. **8**, 1–8 (2017).
36. L. Gudmundsson, J. Boulange, H. X. Do, S. N. Gosling, M. G. Grillakis, A. G. Koutroulis, M. Leonard, J. Liu, H. Müller Schmied, L. Papadimitriou, Y. Pokhrel, S. I. Seneviratne, Y. Satoh, W. Thiery, S. Westra, X. Zhang, F. Zhao, Globally observed trends in mean and extreme river flow attributed to climate change. *Science*. **371**, 1159–1162 (2021).
37. IPCC, "Anthropogenic and Natural Radiative Forcing" in *Climate Change 2013: The Physical Science Basis* (Cambridge Univ. Press, 2013), pp. 659-740.
38. C. E. Iles, G. C. Hegerl, Systematic change in global patterns of streamflow following volcanic eruptions. *Nat. Geosci*. **8**, 838–842 (2015).
39. M. Huss, R. Hock, Global-scale hydrological response to future glacier mass loss. *Nat. Clim. Chang*. **8**, 135–140 (2018).
40. L. Gudmundsson, J. Kirchner, A. Gädeke, J. Noetzli, B. K. Biskaborn, Attributing observed permafrost warming in the northern hemisphere to anthropogenic climate change. *Environ. Res. Lett*. **17** (2022), doi:10.1088/1748-9326/ac8ec2.
41. W. R. Berghuijs, R. A. Woods, M. Hrachowitz, A precipitation shift from snow towards rain leads to a decrease in streamflow. *Nat. Clim. Chang*. **4**, 583–586 (2014).
42. M. G. Floriancic, W. R. Berghuijs, P. Molnar, J. W. Kirchner, Seasonality and Drivers of Low Flows Across Europe and the United States. *Water Resour. Res*. **57**, 1–17 (2021).
43. M. Mudelsee, M. Börngen, G. Tetzlaff, U. Grünewald, No upward trends in the occurrence of extreme floods in central Europe. *Nature*. **425**, 166–169 (2003).
44. J. D. Hunt, E. Byers, Y. Wada, S. Parkinson, D. E. H. J. Gernaat, S. Langan, D. P. van Vuuren, K. Riahi, Global resource potential of seasonal pumped hydropower storage for energy and water storage. *Nat. Commun*. **11**, 1–8 (2020).
45. N. L. Poff, J. D. Olden, D. M. Merritt, D. M. Pepin, Homogenization of regional river dynamics by dams and global biodiversity implications. *Proc. Natl. Acad. Sci. U.S.A.* **104**, 5732–5737 (2007).

46. L. Gudmundsson, H. X. Do, M. Leonard, S. Westra, The Global Streamflow Indices and Metadata Archive (GSIM) - Part 2: Time Series Indices and Homogeneity Assessment. *PANGAEA*, doi: https://doi.org/10.1594/PANGAEA.887470 (2018).
47. G. Ghiggi, L. Gudmundsson, V. Humphrey, G-RUN: Global Runoff Reconstruction. figshare. doi: https://doi.org/10.6084/m9.figshare.9228176.v2 (2019).
48. U. Schneider, S. Hänsel, P. Finger, E. Rustemeier, M. Ziese, GPCC Full Data Monthly Product Version 2022 at 2.5°: Monthly Land-Surface Precipitation from Rain-Gauges built on GTS-based and Historical Data. doi: https://doi.org/10.5676/DWD_GPCC/FD_M_V2022_250 (2022).
49. M. Cucchi, G. P. Weedon, A. Amici, N. Bellouin, S. Lange, H. Müller Schmied, H. Hersbach, C. Cagnazzo, C. Buontempo, Near surface meteorological variables from 1979 to 2019 derived from bias-corrected reanalysis, version 2.1. doi: https://doi.org/10.24381/cds.20d54e34.
50. J. Muñoz Sabater, ERA5-Land hourly data from 1950 to present. *Copernicus Climate Change Service (C3S) Climate Data Store (CDS)*, doi: https://doi.org/10.24381/cds.68d2bb30 (2019).

Acknowledgements:

Funding: This study has been supported by the National Natural Science Foundation of China (grant no. 42361144001), the Strategic Priority Research Program of the Chinese Academy of Sciences (grant no. XDA20060402), the Shenzhen Science and Technology Program (KCXFZ20201221173601003), the Henan Provincial Key Laboratory of Hydrosphere and Watershed Water Security, and funding from the School of Geography and water@leeds at the University of Leeds.

Author contributions: J.L., H.W., M.K., and J.H. conceived and designed the study. H.W. conducted the analyses, and drafted the paper, all under the supervision of J.L., M.K., and J.H. All authors contributed to data interpretation and provided substantive revisions on the manuscript.

Competing interests: The authors declare no competing interests.

Data availability: The river flow time series from GSIM can be downloaded from DOI: 10.1594/PANGAEA.887470 (*46*). The runoff reconstruction dataset GRUN is available from DOI: 10.6084/m9.figshare.9228176.v2 (*47*). The model results are available from the ISIMIP2b project in Water (global) sector (https://www.isimip.org/outputdata/). Other data are presented in the supplementary materials. The streamflow time series from the GRDC are available at https://www.bafg.de/GRDC. The observed monthly GPCC precipitation is available at DOI: 10.5676/DWD_GPCC/FD_M_V2022_250 (*48*). The CRUTEM5 dataset is available at https://www.metoffice.gov.uk/hadobs/crutem5/data/CRUTEM.5.0.1.0/download.html. The CPC soil moisture data can be downloaded from www.esrl.noaa.gov/psd. The bias-corrected reanalysis WFDE5 and ERA5 monthly land data can be downloaded from CDS website [WFDE5: available at DOI: 10.24381/cds.20d54e34 (*49*). ERA5: available at DOI: 10.24381/cds.68d2bb30 (*50*)]

Supplementary Materials

This PDF file includes:

Materials and Methods

Figs. S1 to S18